ARTICLE

Critical Size of Crystalline ZrO_2 Nanoparticles Synthesized in Near- and Supercritical Water and Supercritical Isopropyl Alcohol

Jacob Becker,[†] Peter Hald,[†] Martin Bremholm,[†] Jan S. Pedersen,[†] Jacques Chevallier,[‡] Steen B. Iversen,[§] and Bo B. Iversen[†,*]

[†]Department of Chemistry and Interdisciplinary Nanoscience Center and [‡]Department of Physics, University of Aarhus, DK-8000 Aarhus, Denmark, and [§]SCF Technologies a/s, Smedeholm 13, DK-2730 Herlev, Denmark

ABSTRACT Nanocrystalline ZrO_2 samples with narrow size distributions and mean particle sizes below 10 nm have been synthesized in a continuous flow reactor in near and supercritical water as well as supercritical isopropyl alcohol using a wide range of temperatures, pressures, concentrations and precursors. The samples were comprehensively characterized by powder X-ray diffraction (PXRD), transmission electron microscopy (TEM), and small-angle X-ray scattering (SAXS), and the influence of the synthesis parameters on the particle size, particle size distribution, shape, aggregation and crystallinity was studied. On the basis of the choice of synthesis parameters either monoclinic or tetragonal zirconia phases can be obtained. The results suggest a critical particle size of 5−6 nm for nanocrystalline monoclinic ZrO_2 under the present conditions, which is smaller than estimates reported in the literature. Thus, very small monoclinic ZrO_2 particles can be obtained using a continuous flow reactor. This is an important result with respect to improvement of the catalytic properties of nanocrystalline ZrO_2.

KEYWORDS: nanoparticles · critical size · supercritical fluids · zirconia · particle size and size distribution

Zirconia systems have attracted a lot of attention due to their extensive use within a wide range of fields such as ceramics,[1] catalysis,[2,3] chromatographic materials,[4,5] fuel cell technology,[6,7] and gas sensor applications.[8−10] Many applications of zirconia require the high-temperature tetragonal and cubic phases, which are normally stable only at temperatures above 1200 and 2400 °C, respectively. Stabilization of zirconia is commonly achieved through doping with, for example, Ce, Y, or Sc,[11−13] and the synthesis and properties of such mixed oxides has therefore been a major field of research. Alternatively, particle-size stabilization has been utilized for the high-temperature phases. When the sizes of the crystallites decrease, the relative contributions of various energy factors change and the tetragonal phase becomes stable. Garvie studied the phase stability of nanocrystalline zirconia phases and estimated that the critical size is about 10 nm.[14] Between 11 and 30 nm the tetragonal and monoclinic phases co-exist, but above approximately 30 nm phase pure monoclinic samples are obtained. The critical size of zirconia was recently reviewed by Shukla and Seal,[15] who supported the Garvie value of 10 nm although the estimate is dependent on conditions such as nonaggregated particles and ambient temperature and pressure.

Here we report on the synthesis of nanocrystalline zirconia in near- and supercritical water (SCW) as well as supercritical isopropyl alcohol (SCIP) using a wide range of temperatures, pressures, concentrations, and precursors. This allows systematic investigation of solvent and precursor effects on the particle formation in a continuous flow supercritical synthesis reactor. The critical point of water is at 374.1°C and 221 bars, while that of isopropyl alcohol is at 258°C and 58 bar. The present synthesis products were extensively characterised not only by powder X-ray diffraction (PXRD) and transmission electron microscopy (TEM), but also by small angle X-ray scattering (SAXS).[16] SAXS provides estimates of both *particle* size and size distribution, which is complementary to the *crystallite* size estimates obtained by PXRD. The experimental results lead to a new estimate of critical particle size for tetragonal ZrO_2 as well as discussion of what factors influence the phase stabilization in the present media. Synthesis of cubic zirconia in supercritical water has been reported by Arai and co-workers,[17,18] who used a $ZrOCl_2$ precursor, temperatures of 400−490 °C and a pressure of 30 MPa, resulting in spherical

*Address correspondence to bo@chem.au.dk.

Received for review September 19, 2007 and accepted April 20, 2008.

Published online May 10, 2008.
10.1021/nn7002426 CCC: $40.75

particles with a size of ~10 nm. The crystal phase was reported to be cubic. Similar studies have been performed by Sue and co-workers,[19] who used a $ZrO(NO_3)_2$ precursor to study particle size, crystallinity, and conversion efficiency on the conceptual basis of metal oxide solubility and supersaturation.

RESULTS AND DISCUSSION

ZrO_2 Phase Contents. All ZrO_2 synthesis products consisted of a mixture of tetragonal and monoclinic ZrO_2 (*t*-ZrO_2 and *m*-ZrO_2, respectively) in varying ratios. It is straightforward to monitor the phase variations since the tetragonal phase has a large single peak at $2\theta = 30.11°$, whereas the monoclinic phase has two equal peaks located at $2\theta = 28.20°$ and 31.49°. Figure 1a−g displays PXRD data for ZrO_2 synthesized in water, while Figure 2 shows corresponding data for the ZrO_2 synthesized in SCIP. For nanocrystalline samples containing a mixture of phases the two monoclinic peaks will be seen as shoulders on the tetragonal peak. The phase content was only monitored in a qualitative fashion, and no quantitative estimates, for example, from Rietveld analysis were made. The tetragonal and the cubic phases have similar PXRD patterns, and line broadening makes distinction very difficult. The identification of the tetragonal phase is thus based on the literature which reports almost exclusively on tetragonal ZrO_2 for particles in size regimes similar to the present sample.[15] If a distinction between the cubic and the tetragonal phase were to be made accurately, it would require a variety of additional techniques, most notably Raman spectroscopy.[20] This is beyond the scope of the present work.

The phase content can be systematically manipulated by changing temperature, pressure, solvent, or precursor, but no completely phase pure ZrO_2 samples were obtained. The data reveal a clear tendency towards higher temperatures resulting in a high content of *m*-ZrO_2, while low temperatures or low pressures results in high *t*-ZrO_2 contents, Figure 1a−g. The phase content correlates well with the variations in particle sizes, with the possible exception of Figure 1f, where several of the SAXS fits were not optimal. Generally, samples containing very small particles are always rich in *t*-ZrO_2, while samples containing larger particles are rich in *m*-ZrO_2.

ZrO_2 Particle Sizes. For the 0.55 M synthesis series with $Zr(ac)_4$ precursor the Scherrer estimates of the particle sizes were found to range between 4.7−6.8 nm, Table 1. This size range is slightly lowered to 3.8−6.0 nm when the residence is increased and the precursor concentration decreased to 0.11 M, Table 2. The size estimates obtained from PXRD are in excellent agreement with the TEM results. Representative examples of TEM images and some corresponding size distributions are shown in Figure 3a,b. The TEM images reveal some degree of agglomeration in both the 0.55 and the 0.11 M products.

In general there is also very good agreement between the volume weighted average sizes determined from PXRD and SAXS with the SAXS estimates being slightly larger. This presumably reflects that there is a small amorphous fraction, which makes the particle size larger than the crystallite size. In case of ZrO_2 particles synthesized in SCIP there is a slight discrepancy with the PXRD estimate being larger than the SAXS estimate. However, for these samples the number-weighted averages almost equal the volume-weighted averages since the polydispersities are very low. As explained below, the estimates of the polydispersity may in these cases be too low due to fuzzy particle boundaries.

The particle sizes in the samples containing the most *m*-ZrO_2 are substantially smaller than the critical particle size of 10 nm suggested by Garvie, and it is noteworthy that the size distributions do not even overlap 10 nm. From a technological point of view this is highly attractive, since the present synthesis method makes continuous production of extremely small *monoclinic* ZrO_2 particles possible, for example for catalysis purposes, and avoids the phase transformation to tetragonal ZrO_2. Successful synthesis of very small particles of monoclinic ZrO_2 (~6 nm) have been reported earlier by Morgan;[21] however, the synthesis route involved heating of a precursor mixture at 150°C in the bomb for 14 days, and the technique is unlikely to be suitable for industrial applications.

ZrO_2 Agglomeration. A change of solvent and precursor has a dramatic effect on the degree of agglomeration. Figure 4 shows the TEM image of a representative SCIP synthesis product next to the TEM image of a product synthesized in water at similar temperature and pressure. For the SCIP synthesis products, the data indicate particle sizes of 3.6−3.9 nm (PXRD), which was also confirmed by dark-field TEM (data not shown). However, as seen in Figure 4, these very small particles cluster into dense agglomerates. The agglomerates are believed to have formed outside the hot-zone of the synthesis apparatus *after* completion of reactions. Otherwise the small particles presumably would have fused into larger particles. The SCIP ZrO_2 agglomerates are dense enough to yield the two-step SAXS data profile shown in Figure 5, which is very different from the SAXS profiles of all the other products. The two "steps" on the SCIP ZrO_2 SAXS data profile is a direct consequence of the agglomerates, which are dense enough to be regarded as pseudoparticles. The information about these particle aggregates is contained within the first "step" of the curve, while the second step contains the size distribution information of the individual particles.

ZrO_2 Polydispersities. Apart from the mean particle size, the polydispersity is the most important information obtained from the SAXS data. In the present study a Schultz−Zimm distribution was chosen to model the

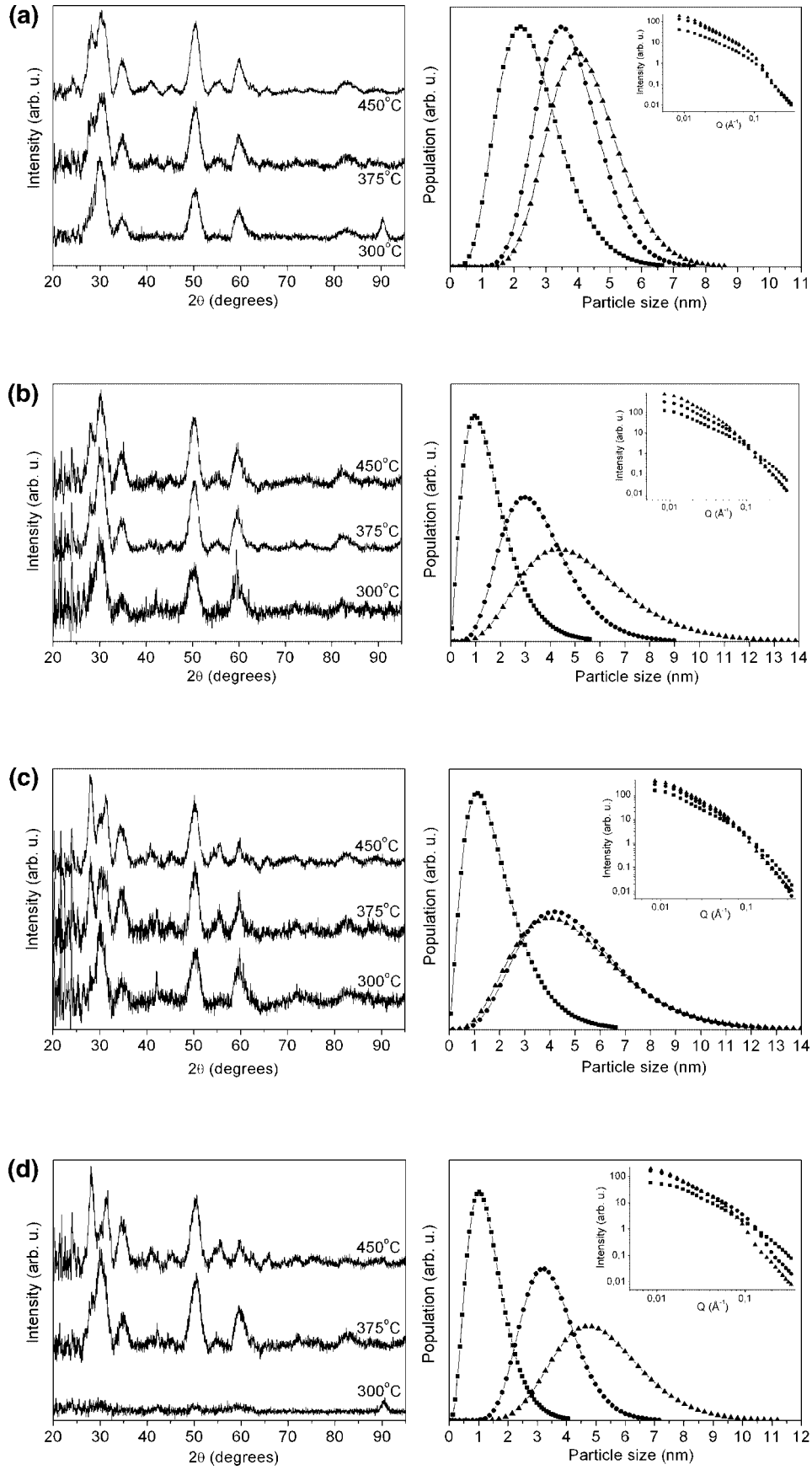
(a)
Intensity (arb. u.)
450°C
375°C
300°C
20 30 40 50 60 70 80 90
2θ (degrees)
Population (arb. u.)
0 1 2 3 4 5 6 7 8 9 10 11
Particle size (nm)
Intensity (arb. u.)
100 10 1 0,1 0,01
0,01 0,1
Q (Å⁻¹)
(b)
Intensity (arb. u.)
450°C
375°C
300°C
20 30 40 50 60 70 80 90
2θ (degrees)
Population (arb. u.)
0 1 2 3 4 5 6 7 8 9 10 11 12 13 14
Particle size (nm)
Intensity (arb. u.)
100 10 1 0,1 0,01
0,01 0,1
Q (Å⁻¹)
(c)
Intensity (arb. u.)
450°C
375°C
300°C
20 30 40 50 60 70 80 90
2θ (degrees)
Population (arb. u.)
0 1 2 3 4 5 6 7 8 9 10 11 12 13 14
Particle size (nm)
Intensity (arb. u.)
100 10 1 0,1 0,01
0.01 0,1
Q (Å⁻¹)
(d)
Intensity (arb. u.)
450°C
375°C
300°C
20 30 40 50 60 70 80 90
2θ (degrees)
Population (arb. u.)
0 1 2 3 4 5 6 7 8 9 10 11 12
Particle size (nm)
Intensity (arb. u.)
100 10 1 0,1 0,01
0.01 0,1
Q (Å⁻¹)

1

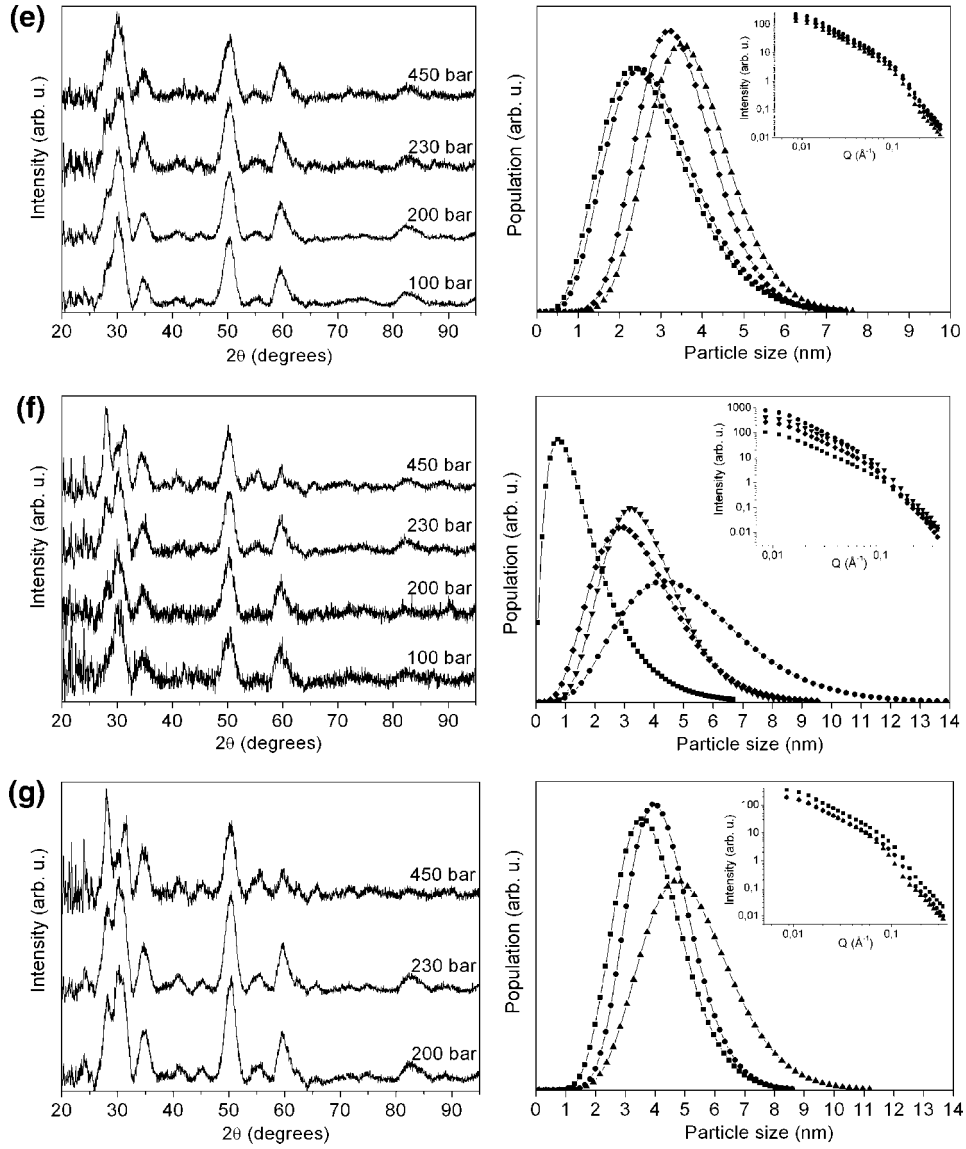

Figure 1 Continued. (a) PXRD data, particle size distributions, and raw data from SAXS of pure-ZrO_2 products synthesized in water at 230 bar with 0.11 M $Zr(ac)_4$ precursor at 300 (■), 375 (●), and 450 °C (▲). (b) PXRD data, particle size distributions, and raw data from SAXS of pure-ZrO_2 products synthesized in water at 230 bar with 0.55 M $Zr(ac)_4$ precursor at 300 (■), 375 (●), and 450 °C (▲). (c) PXRD data, particle size distributions, and raw data from SAXS of pure-ZrO_2 products synthesized in water at 450 bar with 0.55 M $Zr(ac)_4$ precursor at 300 (■), 375 (●), and 450 °C (▲). (d) PXRD data, particle size distributions, and raw data from SAXS of pure-ZrO_2 products synthesized in water at 450 bar with 0.11 M $Zr(ac)_4$ precursor at 300 (■), 375 (●), and 450 °C (▲). The 300 °C product contains predominantly amorphous ZrO_2, possibly because the residence time has been too short for crystallinity to be achieved at the relatively low temperature. (e) PXRD data, particle size distributions, and raw data from SAXS of pure-ZrO_2 products synthesized in water at 375 °C with 0.11 M $Zr(ac)_4$ precursor at 100 (■), 200 (●), 230(▲), and 450 bar (♦). (f) PXRD data, particle size distributions, and raw data from SAXS of pure-ZrO_2 products synthesized in water at 450 °C with 0.55 M $Zr(ac)_4$ precursor at 100 (■), 200 (●), 230 (▲), and 450 bar (♦). Note, however, that several of these SAXS fits were less than satisfactory, and as such the resulting size distributions are not completely reliable. (g) PXRD data, particle size distributions, and raw data from SAXS of pure-ZrO_2 products synthesized in water at 450 °C with 0.11 M $Zr(ac)_4$ precursor at 200 (■), 230 (●), and 450 bar (▲).

particle size distributions.[22] The polydispersity measures the broadness and the degree of asymmetry of the size distribution. Physically it is a measure of the homogeneity (in size and shape) of the particles. At very low values (from 0 to approx. 0.1) the particles may be called monodisperse being extremely homogenous in size and shape. Values of up to approximately 0.5−0.6 indicate ordered particle formation and high homogeneity. At values around 1 the particle sizes are considered random. Polydispersity may also be characterized by the moment relations $\mu_1 = \langle D^3\rangle^{1/3}\langle D^{-1}\rangle$ and $\mu_3 = \langle D^1\rangle/\langle D^3\rangle^{1/3}$ that have been used by Shah *et al.*[23] to identify the growth mode of nanoparticles, Condensation of atoms or small oligomers onto particles results in small polydispersities and $\mu_1 \approx \mu_3 \approx 1$, whereas collision and aggregation of small particles into larger ones gives a broad size distribution with $\mu_1 > 1.25$ and $\mu_3 < 0.905$.[24]

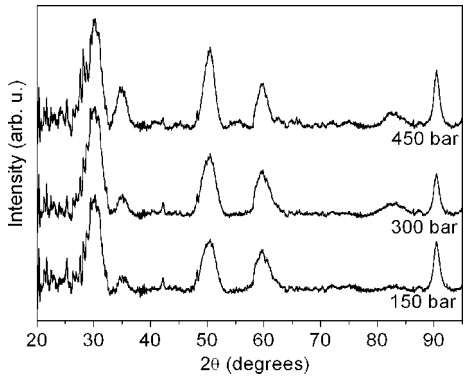

Figure 2. PXRD diffractograms of ZrO_2 synthesized in supercritical isopropyl alcohol (SCIP) at 400 °C with 0.015 M $Zr(CH_3CH_2OH)_4$ precursor.

We observe that by controlling the precursor concentration and/or the flow rate, it is possible to control the polydispersity of the resulting particles. In the 0.55 M synthesis series with $Zr(ac)_4$ precursor, the average polydispersity is 0.52, and it falls within the range of 0.36 to 0.64 except of a single case with 0.75. The corresponding values of μ_1 and μ_3 indicate, according to Shah *et al.*,[23] a particle growth governed by collision and aggregation. However, upon reduction of the $Zr(ac)_4$ concentration and prolongation of residence time, *all* polydispersity values decrease, and the average polydispersity is 0.34 ranging from 0.26 to 0.54. Correspondingly, values of μ_1 decrease and μ_3 values increase, suggesting that particle formation by condensation plays a larger role at these synthesis conditions. This effect may be attributable to either (i) the increased distance between $Zr(ac)_4$ molecules on an atomic scale, which could hinder the formation of irregular primary particles within the time frame which is available before all reactant is exhausted (concentration effect), or (ii) the prolonged residence time, which could homogenize the particles through a ripening process. Residence times calculated from medium densities are given in Table 1 and Table 2.

Overall, the polydispersities are found to decrease as the temperature is raised. As residence times in general are substantially shorter at elevated temperatures, it may

TABLE 1. Temperature and Pressure Parameters for the Synthesis with 0.55 M $Zr(ac)_4$ Precursor in Water[a]

					SAXS				
T (°C)	P (bar)	density[b] (g/cm^3)	residence time (s)	PXRD $\langle D\rangle_{vol}$ (nm)	D_{mean} (nm)	$\langle D\rangle_{vol}$ (nm)	μ_1	μ_3	poly-dispersity
300	100	0.715	21		1.1	2.91	2.14	0.76	0.62
300	200	0.735	22		1.3	3.29	1.98	0.77	0.59
300	230	0.738	22		1.7	4.37	2.03	0.77	0.60
300	450	0.771	23	4.8	1.9	5.16	2.26	0.75	0.64
375	100	0.041	1.3	5.2	3.1	5.76	1.36	0.87	0.40
375	200	0.121	3.6		3.9	8.62	1.62	0.82	0.50
375	230	0.164	4.9		3.5	6.38	1.34	0.88	0.39
375	450	0.614	18		4.8	8.76	1.34	0.88	0.39
450	100	0.034	1.0	4.7	1.7	5.29	3.21	0.69	0.75
450	200	0.079	2.4		3.7	6.37	1.29	0.89	0.36
450	230	0.090	2.7		5.2	10.02	1.41	0.86	0.42
450	450	0.343	10	6.8	3.5	6.87	1.43	0.86	0.43

[a]The PXRD volume averaged size estimates have been corrected for instrumental broadening using a Gaussian model for the peak widths W ($W^2_{total} = W^2_{particle} + W^2_{inst}$). [b]Densities were taken from "Thermodynamic Properties of Water: Tabulation from the IAPWS Formulation 1995 for the Thermodynamic Properties of Ordinary Water Substance for General and Scientific Use", Allan H. Harvey, October 1998.

TABLE 2. Temperature and Pressure Parameters for the Synthesis with 0.11 M $Zr(ac)_4$ Precursor in Water[a]

					SAXS				
T (°C)	P (bar)	density[b] (g/cm^3)	residence time (s)	PXRD $\langle D\rangle_{vol}$ (nm)	D_{mean} (nm)	$\langle D\rangle_{vol}$ (nm)	μ_1	μ_3	poly-dispersity
300	100	0.715	61		1.8	4.23	1.76	0.80	0.54
300	200	0.735	62		3.3	5.46	1.25	0.90	0.34
300	230	0.738	63		2.6	4.74	1.34	0.88	0.39
300	450	0.771	65		1.4	3.09	1.62	0.82	0.50
375	100	0.041	3.5		2.8	5.20	1.36	0.87	0.40
375	200	0.121	10		2.9	5.19	1.32	0.88	0.38
375	230	0.164	14	4.0	3.8	5.35	1.14	0.94	0.26
375	450	0.614	52		3.5	5.03	1.15	0.93	0.27
450	200	0.079	6.7	4.0	3.9	5.96	1.19	0.92	0.30
450	230	0.090	7.6	3.8	4.3	6.06	1.14	0.94	0.26
450	450	0.343	29	6.0	5.2	7.79	1.18	0.93	0.29

[a]The PXRD volume averaged size estimates have been corrected for instrumental broadening using a Gaussian model for the peak widths W ($W^2_{total} = W^2_{particle} + W^2_{inst}$). [b]Densities were taken from "Thermodynamic Properties of Water: Tabulation from the IAPWS Formulation 1995 for the Thermodynamic Properties of Ordinary Water Substance for General and Scientific Use", Allan H. Harvey, October 1998.

be postulated that short residence time led to a low polydispersity. However, a number of exceptions from this trend is observed, most notably the syntheses at [375 °C, 450 bar] and [450 °C, 450 bar] in the 0.11 M precursor concentration series. Here the residence times are quite long (52 and 29 seconds, respectively) but these conditions still yield some of the lowest polydispersities. Likewise, the [375 °C, 450 bar, 0.55 M] synthesis has a residence time of 18 seconds and a polydispersity of 0.39, which is one of the lowest observed in this concentration series (Table 1). On contrast the [300 °C, 100 bar, 0.55 M] synthesis has a very high polydispersity of 0.62 despite the comparable residence time of 21 seconds. On the basis of these observations, it seems that temperature rather than residence time explains the observed trends in polydispersity within a single precursor concentration series.

The ZrO_2 particles resulting from the SCIP syntheses are particularly interesting since the polydispersities were found to be less than 0.025 in all cases, which normally is interpreted as monodispersity. However, potential inaccuracies in the polydispersities must be taken into account. Since the data do not extend to very high *q*-values, a precise determination of the polydispersities is impossible. If the particles do not have sharp particle boundaries within the agglomerates, this would result in a sharp decrease of intensity at high *q*-values. Such a drop in intensity is *also* a sign of a low polydispersity, and the SAXS modelling is unable to differentiate between the two cases. The fact that for the SCIP synthesis the volume averaged SAXS particle size estimates are slightly smaller than PXRD crystallite size estimates indicates that there is some effect of fuzzy boundaries for these very small particles. Nevertheless, it is clear that the SCIP syntheses have produced much more homogenous particles than the SCW syntheses.

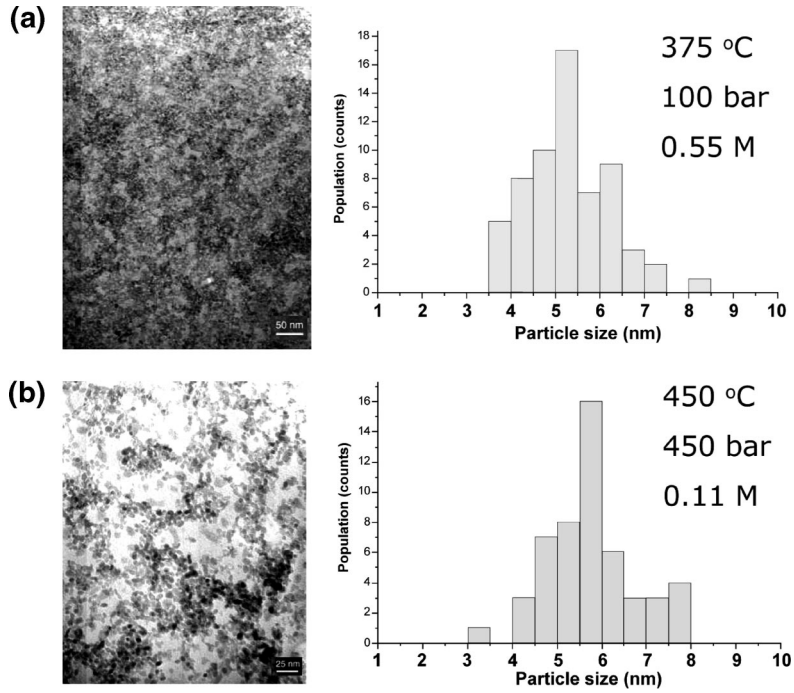

Figure 3. (a) TEM-derived particle size distributions of ZrO_2 synthesized in water from $Zr(ac)_4$. (b) 450 °C, 450 bar and 0.11 M precursor concentration.

Effects of Temperature, Pressure, and Residence Time on ZrO_2 Synthesis. The SAXS-determined size distributions in Figure 1a−d show a steady progression towards larger particle sizes as the temperature is raised. The size distributions also broaden as the temperature is raised. Furthermore, as the temperature is raised and the particle sizes increase, the PXRD patterns show a progression of phase contents from *t*-ZrO_2 to *m*-ZrO_2. Thus, a high synthesis temperature favours the monoclinic phase, and temperature therefore provides control over the phase contents.

As for the pressure, the tendencies are less clear. The pressure has a large effect on the medium density, which in turn influences the residence time. The densities and residence times are given in Table 1 and Table 2. The residence time has a large variation between different synthesis runs ranging from a few seconds to more than a minute. At temperatures above 300 °C, where the density and residence time variations are most pronounced, no trends in particle size, crystallinity or phase contents are found. It seems that at high synthesis temperatures, the residence time is not a factor of great importance; crystallization is achieved instantly, and the particles obtain almost full size and reach a "slow growth" regime within seconds. At 300 °C the compressibility of water is relatively low, and as such the observed pressure effects can hardly be explained in terms of medium density.

Generally, it is important to separate effects of pressure from effects of density. In the present experiments, it is evident that low pressure favors small particle sizes, which again corresponds to a high content of the tetragonal phase, Figure 1e−g. This trend is observed despite the fact that residence time varies from approx. 1 second (at 450 °C) to more than a minute (at 300 °C), although one may argue that the combination of low temperature/long residence time and high temperature/short residence time could lead to similar particle sizes. One would expect that high pressure favors larger particle sizes and the monoclinic phase, but this is not the case. Supercritical conditions seem to *stabilize* the formation of the monoclinic phase. Thus, the most phase-pure content of monoclinic ZrO_2 is obtained at high temperatures *and* high pressures as seen in Figure 1c,d. The temperature seems to be the dominant factor for the particle size and phase contents.

Pressure effects are most pronounced at low temperatures (300 °C). Evidence for this is given in the 300 °C temperature series for the 0.55 M $Zr(ac)_4$ precursor.

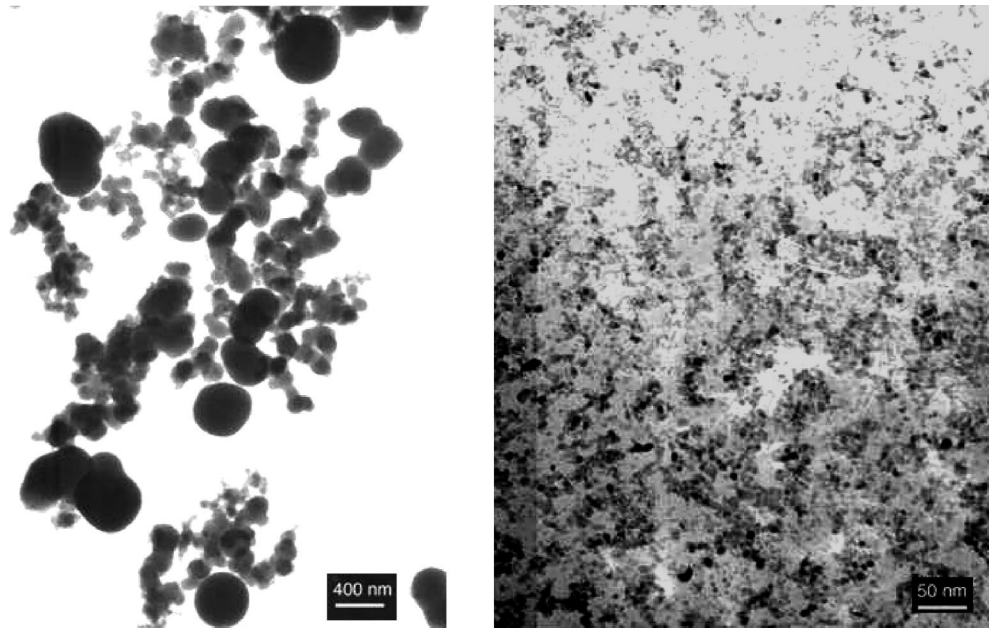

Figure 4. TEM images of ZrO_2 synthesized in SCIP at 400 °C, 450 bar with 0.015 $Zr(CH_3CH_2OH)_4$ precursor and ZrO_2 synthesized in water at 375 °C, 450 bar with 0.55 M $Zr(ac)_4$ precursor.

Here, the degree of crystallinity increases with increasing pressure, Figure 6a, a trend which in turn seems to follow a progression in particle sizes. However, both effects vanish when temperature is raised. The pressure induced crystallization also disappears when the concentration is reduced and the residence time is prolonged (from ~20 seconds to ~60 seconds). Thus, a longer residence time in the hot reactor gives more time for crystallization. This is demonstrated with the samples from the 300 °C series with 0.11 $Zr(ac)_4$ precursor, Figure 6b, which are all crystalline except for the 450 bar outlier sample. As it is seen from the corresponding size distributions, the nice progression of particle sizes has been suppressed.

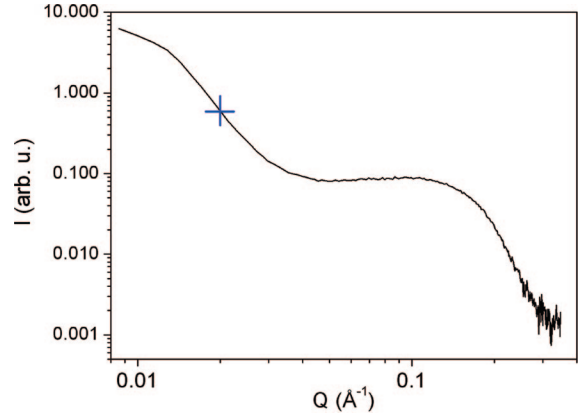

Figure 5. SAXS raw-data profile of the ZrO_2 synthesized in SCIP at 400 °C and 300 bar with 0.015 M $Zr(CH_3CH_2OH)_4$ precursor. The first of the two "steps" on the curve (from the left) is associated with the agglomeration of these ZrO_2 particles , and the second one is associated with the sizes of the particles themselves. As we were interested in the latter information, the data fit was initiated at the cross.

The ZrO_2 samples synthesised in SCIP only contain very small amounts of *m*-ZrO_2. This is in good agreement with the very small particle sizes obtained under these conditions. Once more pressure seems to favor the smallest particle sizes (Table 3).

ZrO_2 Critical Particle Size. The idea that there exists a certain critical particle size which constitutes a limit of stability between *t*-ZrO_2 and *m*-ZrO_2 was first proposed by Garvie in 1965,[25] based on experiments done by Clearfield.[26] The critical particle size stems from the difference in the surface energy of the two ZrO_2 polymorphs, with *t*-ZrO_2 being lowest. This means that if the relative surface area gets large enough, that is, if the particle size gets small enough, then the *t*-ZrO_2 phase will be stabilized. Garvie originally proposed the critical particle diameter to be 30 nm at 300 °C,[25] but later revised the value to 10 nm at room temperature.[14] Since then there has been considerable discussion on the subject, and other groups have argued that stabilization of *t*-ZrO_2 could also be due to, for instance, strain from internal hydrostatic pressures (Gibbs−Thompson effect), structural similarities between the amorphous and tetragonal phases, water vapor (as this changes the interfacial energies between particles), and anions bound on the particle surfaces or embedded in the ZrO_2 matrix as well as other factors. An extensive overview of the subject was given by Shukla and Seal.[15] The fact that it is possible to make *t*-ZrO_2 particles with diameters of more than 100 nm certainly indicates that the *t*-ZrO_2 stabilization is affected by other factors than just surface area.[27,28] This point is stressed by Shukla and Seal,[15] who proceed to the important conclusion that no single phase stabilization mechanism satisfactorily explains all the data on the stabilization of high-

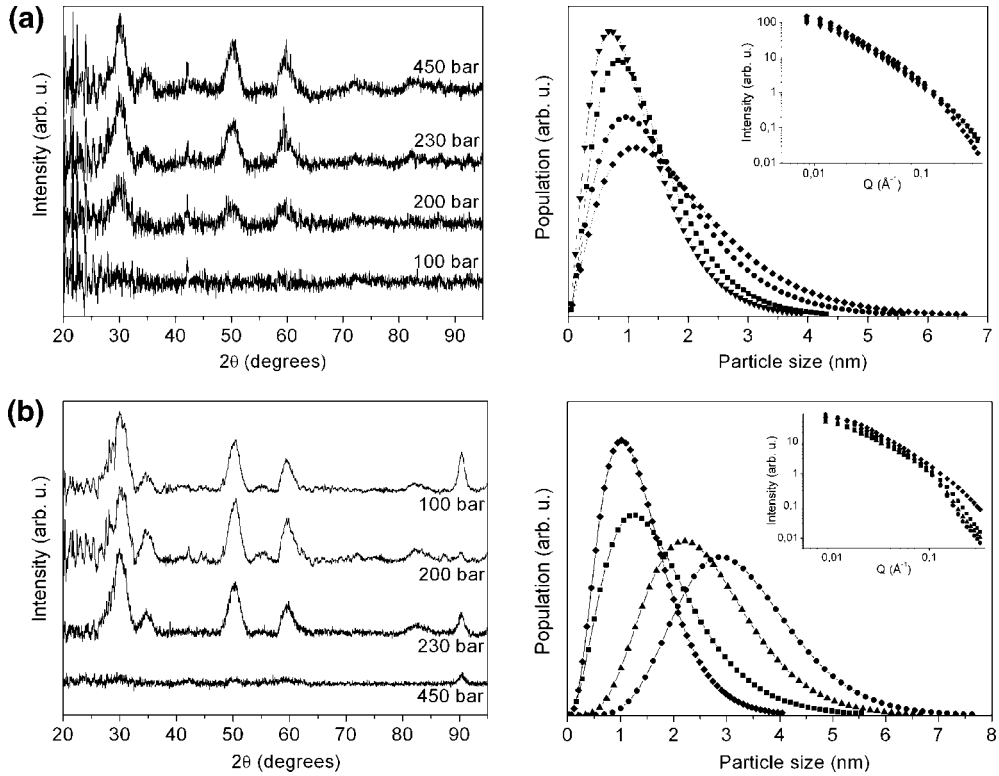

Figure 6. (a) PXRD data, size distributions, and raw data from SAXS for the pure ZrO_2 samples synthesized in water at 300 °C with 0.55 M $Zr(ac)_4$ precursor at 100 bar (▼), 200 bar (■), 230 bar (●), and 450 bar (♦). (b) PXRD data, size distributions, and raw data from SAXS for the pure ZrO_2 samples synthesized in water at 300 °C with 0.11 M $Zr(ac)_4$ precursor at 100 bar (■), 200 bar (●), 230 bar (▲), and 450 bar (♦).

temperature ZrO_2-phases. Since other factors besides particle size have influence on the stability of *t*-ZrO_2, the observed value of the critical size is dependent on the specific route of synthesis.[29] A particular route of synthesis will introduce specific stresses, impurities, *etc.* in the products. It is therefore of interest to compare synthesis in SCW and SCIP with the other routes of syntheses from the literature.

The present work offers some support to the theory of critical particle size, at least as far as the overall trends are concerned. First of all, the theory explains the previous-mentioned progression in phase contents from *t*-ZrO_2 to *m*-ZrO_2 with increasing particle size. Secondly, it explains why it has been impossible to completely isolate a single phase of ZrO_2. If the size distributions of the particles are overlapping the critical value, it will inevitably lead to two phases in the product. With this in mind, we have attempted to extract a value of the critical particle size from our results. Figure 7 shows the SAXS-derived size distributions for the ZrO_2-products which contained the most *t*-ZrO_2 and *m*-ZrO_2, respectively. The ZrO_2 synthesized at [T = 375 °C, P = 100 bar] was almost pure in *t*-ZrO_2, and the ZrO_2 synthesized at [T = 450 °C, P = 450 bar] was almost pure in *m*-ZrO_2. The critical particle size presumably is located somewhere within the boundaries of these size distribu-

TABLE 3. Temperature and Pressure Parameters for the Synthesis with 0.015 M $Zr(et)_4$ Precursor in Isopropyl Alcohol Mixed with 0.5 % Water[a]

			SAXS				
T (°C)	P (bar)	PXRD $\langle D\rangle_{vol}$ (nm)	D_{mean} (nm)	$\langle D\rangle_{vol}$ (nm)	μ_1	μ_3	poly-dispersity
400	150	3.6	2.5	2.51	1.00	1.00	0.02
400	300	3.4	2.9	2.90	1.00	1.00	0.01
400	450	3.9	5.3	5.30	1.00	1.00	0.01

[a]The PXRD volume averaged size estimates have been corrected for instrumental broadening using a Gaussian model for the peak widths W ($W^2_{total} = W^2_{particle} + W^2_{inst}$).

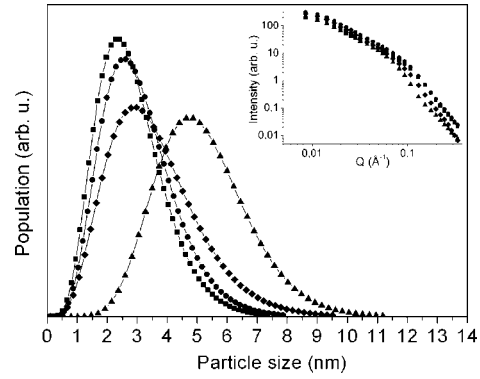

Figure 7. Size distributions and raw data from SAXS for pure ZrO_2 samples synthesized in water, corresponding to the most phase-pure samples of *t*-ZrO_2 and *m*-ZrO_2, as observed in PXRD. The two samples richest in *t*-ZrO_2 were both obtained at [375 °C, 100 bar] with precursor concentrations of 0.11 M (■) and 0.55 M (●), and the two samples richest in *m*-ZrO_2 were obtained at [450 °C, 450 bar] with precursor concentrations of 0.11 M (▲) and 0.55 M (♦).

tions. In other words, the distributions of the samples which are rich in *m*-ZrO_2 should predominantly be located in the size regime above the critical value, and the samples rich in *t*-ZrO_2 should be located below. On the basis of these assumptions, the value which can be extracted from Figure 7 is 5 ± 1 nm. This estimate is of course number weighted, as it is derived from the (number) size distributions produced by SAXS. If weighted by volume, the critical size estimate increases slightly to 6 ± 1 nm. In both cases, the extracted value is substantially smaller than the value of 10 nm which was originally proposed by Garvie. In the extensive review of Shukla and Seal[15] no similarly small value of the critical size is suggested. Shukla and Seal also noted that the value of 10 nm is only applicable for strain free, single domain ZrO_2 nanoparticles of spherical or near-spherical shape in contact with air at ambient pressure and temperature. Aggregation of the nanocrystallites leads to an increase in the critical size to as much as 33 nm. Yet our results suggest a value of less than 10 nm, even though we do observe some particle aggregation (Figure 3a,b).

Assuming that the concept of "critical particle size" is valid, the fact that we obtain a smaller estimate of the critical size leads to a number of possible explanations: (i) Our particles are completely free of internal impurities and strains, and the Garvie value is larger because of small undetected amounts of microstrain, impurities, and other factors affecting the critical particle size. Alternatively, (ii) it could be a thermodynamic effect, as the present particles are synthesized in the temperature regime of 300 °C to 450 °C. If so, one should expect metastable powders, as the phases formed then are thermodynamically disfavored at room temperature. The latter is unlikely since no phase transformations have been observed even after several months of storage. One might speculate that the phases are kinetically stabilized at room temperature, but this seem unlikely as any postheating of the powders (*e.g.*, extra-drying at 80−200 °C) invariably has left the phase contents unaffected. Another possibility (iii) is that oxygen vacancies play a significant role in the stabilization of *t*-ZrO_2 apart from the contribution from surface energy. This is not unreasonable, as it is the introduction of oxygen vacancies which is believed to be responsible for the stabilization of the tetragonal phase when ZrO_2 is doped by small, trivalent cations (*e.g.*, Sc^{3+}, Fe^{3+}, and others). In this particular context, it may then be speculated that the oxygen vacancies are easily eliminated at high temperatures (possibly assisted by high pressures), thus causing a tetragonal-to-monoclinic phase transformation, whereas they remain trapped in the ZrO_2 matrix at lower temperatures or pressures, resulting in a stabilization of the tetragonal phase. Finally (iv) the acetic acid present in the suspensions could influence the surface energy in such a way that the critical particle size is reduced. This is not an unreasonable assumption, since low pH-values have been used in batch synthesis of *m*-ZrO_2 with particle sizes below the critical value of 10 nm.[21]

Upon comparison, it is noted that the particles obtained here at high temperatures (T > 400 °C) are smaller than those obtained by Arai *et al.*[17,18] This may be a result of synthesis temperature, as Arai *et al.* reported temperatures in the range 400−490 °C. It could also be due to the different precursor used ($ZrOCl_2$ *versus* the $Zr(ac)_4$), or maybe simply the synthesis apparatus. The fluid dynamics at the mixing point, and in the reactor as a whole, are believed to have a strong effect on the products.[30]

CONCLUSION

Synthesis of nanocrystalline ZrO_2 has been carried out in near- and supercritical water as well as supercritical isopropyl alcohol. Detailed characterization using PXRD, SAXS, and TEM revealed all samples to be mixtures of *t*-ZrO_2 and *m*-ZrO_2. In general, high temperature and high pressure increases the particle size and the *m*-ZrO_2 content. The synthesis temperature is the key controlling factor for the product, although at subcritical temperatures increasing pressure can induce crystallization. The mixture of phases presumably originates from the particle size distributions of the products overlapping the critical size for *t*-ZrO_2. Almost phase pure *t*-ZrO_2 is obtained at low temperature and pressure, whereas high temperature and pressure leads to almost phase pure *m*-ZrO_2. Synthesis in SCIP gives almost monodisperse products, whereas SCW results in significant polydispersity. It is remarkable that stable *m*-ZrO_2 can be synthesized in minutes under supercritical conditions with an average size of 5 ± 1 or 6 ± 1 nm, depending on whether the average is weighted by number or by volume . This is considerably below previous estimates for the critical size of *t*-ZrO_2, and since *m*-ZrO_2 is an important catalyst, the potential of nanostructuring this phase is of significant technological interest.

METHODS

Synthesis. Synthesis in supercritical media requires a specialized synthesis apparatus, which is capable of handling high temperatures and high pressures, and which furthermore possesses high resistance to corrosion. The synthesis apparatus used in the present study has been described by Hald *et al.*[31] It was constructed with the aim of continuous flow particle synthesis, which is industrially preferred relative to batch processes.

The first series of experiments used SCW with zirconium acetate, $Zr(ac)_4$, as precursor. This is similar to the study of Poliakoff and co-workers.[12] At the temperatures in question, $Zr(ac)_4$ is believed to decompose thermally to $Zr(OH)_4$, which subsequently eliminates water to form ZrO_2. In the first run a precursor concentration of 0.55 M and a high flow rate (residence times

of 20−30 seconds) was used. Twelve syntheses were carried out by combining temperatures of 300, 375, and 450 °C with pressures of 100, 200, 230, and 450 bar. It should be emphasized, that the temperature of 450 °C was very difficult to maintain with our synthesis apparatus, since large amounts of heat are transported out of the system with the reaction medium when the exit valve is opened. Thus, even though the initial temperature was 450 °C when each synthesis commenced, the actual synthesis temperature was somewhat lower, probably 430 ± 10 °C. Owing to these fluctuations the initial temperature was considered to be the best label for these syntheses. All other synthesis temperatures are constant throughout the syntheses. In addition to the synthesis conditions mentioned above, a few test syntheses were conducted at temperatures below 300 °C, but none of these produced crystalline products (PXRD data not shown). In Table 1 the synthesis conditions and various particle size estimates are summarized.

Next the precursor concentration was changed to 0.11 M, and the flow rate was reduced to give a synthesis speed of 60−80 seconds. The same series of temperature and pressure conditions was used, with the exception of the [450 °C, 100 bar] synthesis. In Table 2 synthesis conditions and size estimates are summarized.

The solvent was then changed to isopropyl alcohol and the precursor was changed to zirconium ethoxide, $Zr(OCH_2CH_3)_4$, $Zr(et)_4$, in a concentration of 0.015 M. To assure complete precursor condensation we added 0.5 wt % (0.277 M) water to the isopropyl alcohol solvent. Nine syntheses were carried out by combining temperatures of 200, 300, and 400 °C with pressures of 150, 300, and 450 bars. However, crystalline particles were not obtained at temperatures below 400 °C (PXRD data not shown). In Table 3 conditions for the 400°C SCIP syntheses as well as size estimates are listed.

Characterization. PXRD data were recorded on a STOE StadiP powder diffractometer at Department of Chemistry, University of Aarhus. A Ge(111) single crystal monochromator was used to produce Cu Kα1 radiation, which was detected with a 40° position sensitive detector. PXRD was used to monitor the degree of crystallinity in the samples, to identify crystal phases, and to estimate the volume-averaged particle sizes using the Scherrer method.[32] The diffraction peaks were fitted to a pseudo-Voigt function. The average particle size determined by PXRD is traditionally termed a volume-averaged size. In terms of a number size distribution $n(D)$ that describes the number of particles with diameter between D and $D + dD$, the volume-averaged particles size is given by

$$\langle D\rangle_{vol}^2 = \frac{\langle D^8\rangle}{\langle D^6\rangle} \quad (1)$$

where $\langle D^m\rangle = \int D^m\, n(d)\, dD$ is the mth moment of the number size distribution.

However, PXRD particle size estimation was only done for selected samples, since the data in some cases were too poor for reliable peak fitting. The PXRD measurements were done on the *as-synthesized* samples. Acetic acid was therefore present in the collected particle suspensions, and this acid does not evaporate completely when the particles are dried (100 °C for 1 hour). The acetic acid was evident from the smell of the dried samples, but also because the samples did not form a fine powder. It is noteworthy that increased measuring time did not improve the PXRD data quality significantly.

Representative samples from each synthesis run were investigated by TEM using a Phillips CM20 transmission electron microscope working at 200 kV. Selected images were used to manually establish size distributions. High resolution TEM was done on some of the samples. The resulting images in all cases revealed that the crystal planes extend to the very edge of the nanoparticles (data not shown), which indicates high crystallinity of the particles.

All synthesis products were investigated with SAXS using a Bruker nanoSTAR instrument. A fractal model assuming polydisperse spherical particles was used for fitting the data,[33] and a Schulz−Zimm function was employed to model the size distribution.[22] These models are consistent with the information obtained from the TEM images. A fractal dimension and a ξ-parameter describing the size of the fractals were thus included to take agglomeration phenomena into accounts. Volume-weighted size estimates were derived from the SAXS distributions using standard methods. Note that in the numerical integration over the number size distribution, 100 points were used and the distribution was truncated at the average size plus four times the standard deviation of the distribution.

REFERENCES AND NOTES

1. Bocanegra-Bernal, M. H.; Torre, S. D. Phase Transitions in Zirconium Dioxide and Related Materials for High Performance Engineering Ceramics. *J. Mater. Sci.* **2002**, *37*, 4947–4971.
2. Kaspar, J.; Fornasiero, P.; Graziani, M. Use of CeO_2-Based Oxides in the Three-Way Catalysis. *Catal. Today* **1999**, *50*, 285–298.
3. Kaspar, J.; Fornasiero, P. Nanostructured Materials for Advanced Automotive De-Pollution Catalysts. *J. Solid State Chem.* **2003**, *171*, 19–29.
4. Nawrocki, J.; Dunlap, C. J.; Carr, P. W.; Blackwell, J. A. New Materials for Biotechnology: Chromatographic Stationary Phases Based on Zirconia. *Biotechnol. Progr.* **1994**, *10*, 561–573.
5. Nawrocki, J.; Rigney, M.; McCormick, A.; Carr, P. W. Chemistry of Zirconia and its Use in Chromatography. *J. Chromatogr. A* **1993**, *657*, 229–282.
6. Mizutani, Y.; Hisada, K.; Ukai, K.; Sumi, H.; Yokoyama, M.; Nakamura, Y.; Yamamoto, O. From Rare-Earth Doped Zirconia to 1 kW Solid Oxide Fuel Cell System. *J. Alloys Comp.* **2006**, *408−412*, 518–524.
7. Ralph, J. M.; Schoeler, A. C.; Krumpelt, M. Materials for Lower Temperature Solid Oxide Fuel Cells. *J. Mater. Sci.* **2001**, *36*, 1161–1172.
8. Maskell, W. C. Progress in the Development of Zirconia Gas Sensors. *Solid State Ionics* **2000**, *134*, 43–50.
9. Riegel, J.; Neumann, H.; Wiedenmann, H.-M. Exhaust Gas Sensors for Automotive Emission Control. *Solid State Ionics* **2002**, *152*, 783–800.
10. Lee, J.-H. Review on Zirconia Air-Fuel Ratio Sensors for Automotive Applications. *J. Mater. Sci.* **2003**, *38*, 4247–4257.
11. Barker, W. W.; Bailey, F. P.; Garrett, W. A High-temperature Neutron Diffraction Study of Pure and Scandia-Stabilized Zirconia. *J. Solid State Chem.* **1973**, *7*, 448–453.
12. Cabañas, A; Darr, J. A.; Lester, E.; Poliakoff, M. A Continuous and Clean One-step Synthesis of Nano-particulate $Ce_{1-x}Zr_xO_2$ Solid Solutions in Near-critical Water. *Chem. Commun.* **2000**, *90*, 1–902.
13. Kim, J.; Myeong, W.; Ihm, S. Characteristics in Oxygen Storage Capacity of Ceria-Zirconia Mixed Oxides Prepared by Continuous Hydrothermal Synthesis in Supercritical Water. *Applied Catal. B* **2007**, *71*, 57–63.
14. Garvie, R. C. Stabilization of the Tetragonal Structure in Zirconia Microcrystals. *J. Phys. Chem.* **1978**, *82*, 218–224.
15. Shukla, S; Seal, S. Mechanisms of Room Temperature Metastable Tetragonal Phase Stabilization in Zirconia. *Int. Mater. Rev.* **2005**, *50*, 45–64.
16. Liang, L.; Xu, Y.; Hou, X.; Wu, D.; Sun, Y.; Li, Z.; Wu, Z. Small-angle X-ray Scattering Study on the Microstructure Evolution of Zirconia Nanoparticles During Calcination. *J. Solid State Chem.* **2006**, *179*, 959–967.
17. Adschiri, T.; Kanazawa, K; Arai, K. Rapid and Continuous Hydrothermal Crystallization of Metal Oxide Particles in Supercritical Water. *J. Am. Ceram. Soc.* **1992**, *75*, 1019–1023.
18. Adschiri, T; Yukiya, H.; Arai, K. Hydrothermal Synthesis of Metal Oxide Fine Particles at Supercritical Conditions. *Ind. Eng. Chem. Res.* **2000**, *39*, 4901–4907.
19. Sue, K.; Suzuki, M.; Arai, K.; Ohashi, T.; Ura, H.; Matsui, K.; Hakuta, Y.; Hayashi, H.; Watanabe, M.; Hiaki, T. Size-Controlled Synthesis of Metal Oxide Nanoparticles with a Flow-thorugh Supercritical Water Method. *Green Chem.* **2006**, *8*, 634–638.

20. Cabañas, A.; Darr, J. A.; Lester, E.; Poliakoff, M. Continuous Hydrothermal Synthesis of Inorganic Materials in a Nearcritical Water Flow Reactor; the One-step Synthesis of Nano-particulate $Ce_{1-x}Zr_xO_2$ ($x = 0-1$) Solid Solutions. *J. Mater. Chem.* **2001**, *11*, 561–568.
21. Morgan, P. E. D. Synthesis of 6-nm Ultrafine Monoclinic Zirconia. *Commun. Am. Ceram. Soc.* **1984**, C-204−C205.
22. Teixeira, J. Small-Angle Scattering by Fractal Systems. *J. Appl. Cryst.* **1988**, *21*, 781–785.
23. Shah, P.S.; Hussain, S.; Johnston, K.P.; Korgel, B.A. Role of Steric Stabilization on the Arrested Growth of Silver Nanocrystals in Supercritical Carbon Dioxide. *J. Phys. Chem. B* **2002**, *106*, 12178–12185.
24. Pich, J.; Friedlander, S.K.; Lai, F.S. The Self-preserving Particle Size Distribution for Coagulation of Brownian Motion - III. Smoluchowski Coagulation and Simultaneous Maxwellian Condensation. *J. Aerosol Sci.* **1970**, *1*, 115–126.
25. Garvie, R. C. The Occurrence of Metastable Tetragonal Zirconia as a Crystallite Size Effect. *J. Phys. Chem.* **1965**, *69*, 1238–1243.
26. Clearfield, A. Crystalline Hydrous Zirconia. *Inorg. Chem.* **1964**, *3*, 146–148.
27. Mitsuhashi, T.; Ichihara, M.; Tatsuke, U. Characterization and Stabilization of Metastable Tetragonal ZrO_2. *J. Am. Ceram. Soc.* **1974**, *57*, 97–101.
28. Shukla, S.; Seal, S.; Vij, R.; Bandyopadhyay, S.; Rahman, Z. Effect of Nanocrystallite Morphology on the Metastable Tetragonal Phase Stabilization in Zirconia. *Nano Lett.* **2002**, *2*, 989–993.
29. Shukla, S.; Seal, S. Thermodynamic Tetragonal Phase Stability in Sol-Gel Derived Nanodomains of Pure Zirconia. *J. Phys. Chem. B* **2004**, *108*, 3395–3399.
30. Lester, E.; Blood, P.; Denyer, J.; Giddings, D.; Azzopardi, B.; Poliakoff, M. Reaction Engineering: The Supercritical Water Hydrothermal Synthesis of Nano-Particles. *J. Supercrit. Fluids* **2006**, *37*, 209–214.
31. Hald, P.; Becker, J.; Bremholm, M.; Pedersen, J. S.; Chevallier, J.; Iversen, S. B.; Iversen, B. B. Supercritical Propanol-Water Synthesis and Comprehensive Size Characterisation of Highly Crystralline Anatase TiO_2 Nanoparticles. *J. Solid State Chem.* **2006**, *179*, 2674–2680.
32. Langford, J. I.; Louër, D. Powder Diffraction. *Rep. Prog. Phys.* **1996**, *59*, 131–234.
33. Pedersen, J. S. A Flux- and Background-Optimized Version of the NanoSTAR Small-Angle X-ray Scattering Camera for Solution Scattering. *J. Appl. Cryst.* **2004**, *37*, 369–380.